Int J CARS (2011) 6:47–57
DOI 10.1007/s11548-010-0474-z

ORIGINAL ARTICLE

Extreme leg motion analysis of professional ballet dancers via MRI segmentation of multiple leg postures

Jérôme Schmid · Jinman Kim · Nadia Magnenat-Thalmann

Received: 11 January 2010 / Accepted: 20 April 2010 / Published online: 13 May 2010

Abstract
Purpose Professional ballet dancers are subject to constant extreme motion which is known to be at the origin of many articular disorders. To analyze their extreme motion, we exploit a unique magnetic resonance imaging (MRI) protocol, denoted as 'dual-posture' MRI, which scans the subject in both the normal (supine) and extreme (split) postures. However, due to inhomogeneous tissue intensities and image artifacts in these scans, coupled with unique acquisition protocol (split posture), segmentation of these scans is difficult. We present a novel algorithm that exploits the correlation between scans (bone shape invariance, appearance similarity) in automatically segmenting the dancer MRI images.
Methods While validated segmentation algorithms are available for standard supine MRI, these algorithms cannot be applied to the split scan which exhibits a unique posture and strong inter-subject variations. In this study, the supine MRI is segmented with a deformable models method. The appearance and shape of the segmented supine models are then re-used to segment the split MRI of the same subject. Models are first registered to the split image using a novel constrained global optimization, before being refined with the deformable models technique.
Results Experiments with 10 dual-posture MRI datasets in the segmentation of left and right femur bones reported accurate and robust results (mean distance error: 1.39 ± 0.31 mm).
Conclusions The use of segmented models from the supine posture to assist the split posture segmentation was found to be equally accurate and consistent to supine results. Our results suggest that dual-posture MRI can be efficiently and robustly segmented.

Keywords Segmentation · Registration · Magnetic resonance imaging · Bone

J. Schmid (✉) · J. Kim · N. Magnenat-Thalmann
MIRALab, University of Geneva, Battelle, Building A,
7 rte de Drize, 1227 Carouge, Switzerland
e-mail: schmid@miralab.ch

Introduction

Professional ballet dancers are subject to constant extreme motions which excessively stress the musculoskeletal structures of their joints and may contribute to the development of pathologies such as osteoarthritis (OA). OA is a common disease of the joint, which mostly yields articular cartilage loss along with changes in other joint structures (bone remodeling, ligamentous and muscular alterations) [1]. In order to understand the underlying causes from such strains on the dancer's joints, it is important to examine the extent of the dancer's movements [2,3] as well as the bones morphology which might explain articular cartilage degeneration [4,5]. The in-vivo examination of the anatomical structures of dancers performing intense postures will undoubtedly support the understanding and diagnosis of their associated pathologies. Therefore, the ability to reconstruct and analyze the musculoskeletal structures is an important requirement to reveal the consequences from repetitive extreme motions performed by the dancers, e.g., in order to validate the femoroacetabular movements which can be a factor of joint degeneration through subluxation and excessive labral deformations [4].

In order to analyze their extreme motion, we exploit a unique magnetic resonance imaging (MRI) protocol [6], denoted as 'dual-posture' MRI, which consists of image pairs of lower limbs consisting of normal (supine) and extreme (split) postures, as illustrated in Fig. 1 where the split posture reveals the maximum extent of the dancer's vertical lower

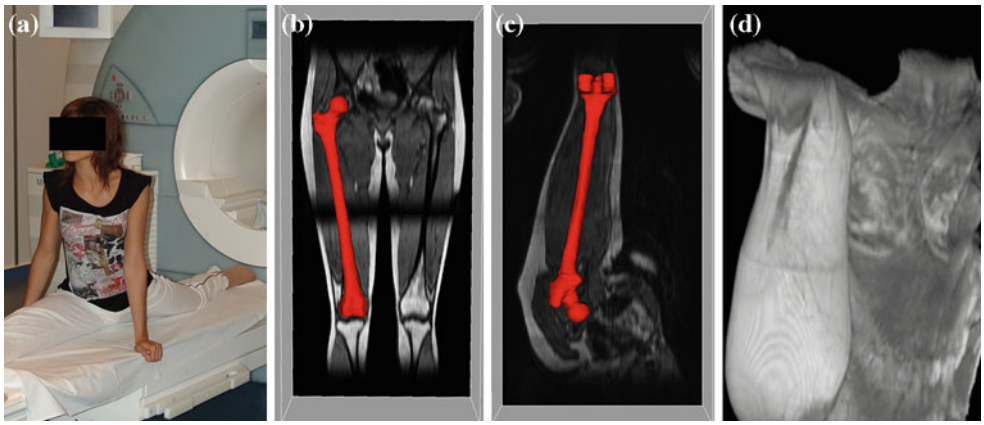

Fig. 1 MRI acquisition: **a** A volunteer dancer before entering MRI scanner in split posture, a coronal slice of a **b** supine and **c** split MRI with bone overlay, **d** volume rendering of a split MRI

limb motion. Such imaging data provide rare insights into the movement of the dancers and enable new observations from the effects of repeated extreme motion and its impact on surrounding anatomical structures. A primary requirement to understand such data is to segment the different musculoskeletal structures, such as soft tissues (e.g., muscles, ligaments, cartilages) and bone tissues (i.e. femur and hip bone) belonging to the hip joint. The segmentation result, for example of the femurs (Fig. 1), enables quantitative motion and morphological analysis to diagnose femoroacetabular impingements [4,5], pre-operative planning or to assist subsequent segmentations of other structures (e.g., cartilages [7,8] or muscles [9] from segmented bones). However, current segmentation practices that rely on manual or semi-automated approaches are subjective, may not be reproducible and are time consuming. There has been several works that attempted to automate the musculoskeletal MRI segmentation [10–13]. However, an automated approach remains a challenging task due to the presence of ubiquitous image artifacts, limited tissue intensity differentiation at joint interfaces caused by proximity of the neighboring bones and their tissue inhomogeneities (e.g., differences cortical/trabecular bone, presence of potential pathologies like osteoporosis and calcifications) [10,14].

In this study, we propose a new segmentation algorithm for dual-posture MRI. We particularly focus our study on professional ballet dancers performing extreme motions (i.e. from supine to split postures). Moreover, the main structure of interest is the femur bone which is a key anatomical structure playing a crucial role in hip joint behavior analysis (e.g., relationship between femoral head sphericity and articular cartilages' OA [5]). Specifically, we aim to segment the femur at two postures in order to investigate the pose changes of the femur between the supine and split postures which can provide quantitative assessment of the subject's extent of motion. The supine posture, which follows standard MRI acquisition protocols (e.g., subject positioning and MRI sequence), can benefit from *a priori* knowledge in terms of appearance (intensity distribution within and around tissues of interest) and organs poses, which facilitates the use of automated methods of bone segmentation. However, due to the largely varying orientations and morphologies between the subjects, and the strong soft tissue deformations evident around the joint areas, the split posture cannot benefit from existing algorithms that are optimized for the standard acquisition. Our research innovates in the automated segmentation of dual-posture MRI by exploiting the characteristics of the femur being a hard tissue (bone) unaffected by changes in postures between the supine and the split. An efficient method to segment the dual-posture MRI is hence proposed where the results from the validated segmentation of the supine MRI are used to assist the segmentation of the split MRI of the same subject.

Related work

Extreme motion analysis

There are significant interests in the field of musculoskeletal disorders such as with OA which affects the joints. Studying the causes of OA is crucial as it commonly affects all people population, particularly the elderly and athletes where it represents a significant economic burden for western societies [15]. For instance, abnormal bone morphology observed as hip femoroacetabular impingements (FAI) is known to be at the origin of early OA [4,5], but there is still some idiopathic OA observed in people who routinely perform extreme motions. A non-invasive way to assess motion is to use medical images in which the structures of interest are acquired at different postures. This is a common approach that has been used in many biomechanical studies [16]. Extreme motion

is defined as the abnormal and excessive movement of the joints and is often found in many elite athletes. The relationship between OA and motion is dependent on various factors, such as the subject characteristics (e.g., gender, age, weight) and performed activities (frequency, intensity) [17]. In some cases, moderate activities might not accelerate the development of OA and may even be beneficial [18]. However, activities with extreme motions have been often associated with an increasing risk for the development of OA.

Our previous studies on professional ballet dancers [2,3] concentrated on the development of subject-specific anatomical models of the hip structures from MRI that were coupled with kinematical data acquired with motion capture. Such in silico simulations enabled the biomechanical effects of extreme movements to be analyzed and put in correlation with radiological observations such as labral tears or femoral neck pits.

Another study [19] from the University of Bern corroborates the idea that athletes participating in intense sports possess a higher rate of hip OA and an earlier onset of this disease compared to the general population. Using karate athletes as subjects, a strong correlation between the early OA and FAI was established.

MRI segmentation of lower limbs

Accurate reconstruction of anatomical models is decisive to understand the bone morphology (changes) and to carry out numerical simulations of the joint biomechanics. This is reflected in the various bone segmentation methods that were proposed, particularly for the major human joints structures (e.g., hip [14,20] and knee [10,13]). Most of these approaches were designed for computed tomography (CT), which inherently attributes excellent contrasts among the bone structures [21–25]. The drawback of CT is its limitation in soft tissue differentiation and in order to acquire the soft and hard tissues simultaneously, MRI is more frequently utilized. With MRI, however, due to intensity differences between cortical and trabecular bone [10] and numerous imagery artifacts (chemical shift, bias field, etc.), the segmentation of the bone structures is more challenging. There have been significant advances in the automated approaches to MRI bone segmentation. In [12] and [26], a region growing algorithm was introduced to segment bones from MRI but manual stages were required (ellipses determination in [12]) or assumptions on the bones location were made [26]. A recent study [27] has demonstrated the use of atlas-based non-rigid registration for MRI musculoskeletal segmentation and muscle action path determination. Alternatively, MRI protocol optimization (magnitude and phase) was presented in [7,13,28] to improve the image quality for subsequent classification/thresholding. Successful bone segmentation was reported using implicit [10,29] and discrete [9,11] deformable models, as well as coupling them with shape priors (e.g., our previous work [20]). Deformable models were shown to be generally more robust to image artifacts (noise, diffused boundaries, etc.) due to the (strong) knowledge on the model shapes (topology, smoothness, shape priors, etc.), given that they are initially relatively close to the structures to be segmented.

These studies aimed at developing segmentation algorithms that were designed for a single posture acquisition using a standard imaging protocol. Thus, the capability of these algorithms for the segmentation of non-standard split MRI may not be applicable (due to, e.g., pose assumptions violated, protocol tuning not possible, etc.). Furthermore, these approaches were not designed to fully use all the information within the dual-posture data of the same patient.

Gilles et al. [30] presented a method for dynamic MRI tracking, which took advantage of the similarity between several postures from the same subject. A first manual initialization was used to segment an initial MRI image. The resulting segmented bone was then manually and coarsely positioned in another MRI with different posture, and its position was eventually refined with a rigid model-to-image registration. Two images were thus ultimately segmented, but the various manual actions seriously hindered the automation and ease of use of the approach.

Methodology

Our proposed segmentation methodology works in two phases—Supine and Split postures—as shown in Fig. 2. For the supine segmentation, an atlas-based registration is used as an initialization for a deformable models method coupled with shape priors. The derived result is then used for the split MRI segmentation as an initialization parameter in a constrained model-to-image registration. A deformable model is again used for further refinements.

Material and pre-processing

MRI acquisitions and ground truth construction

Eleven female dancer subjects (avg.: 18.6 years) were scanned (with consent) using a 1.5-T MRI device (Philips Medical Systems) with the 'VIBE' protocol (Axial 3D T1, TR/TE = 4.15/1.69 ms, FOV/Matrix = 35 cm, 256 × 256, resolution = 1.367 × 1.367 × 5 mm). For each subject, a supine and two split (right and left) MRI were acquired. In the supine posture, both thighs were acquired covering a field-of-view (FOV) from the iliac crests to the beginning of the proximal tibias (Fig. 1b). Dancers entered the scanner in the right and left split posture (Fig. 1a) and were scanned using the same protocol, producing the 'split' datasets (Fig. 1c, d). The

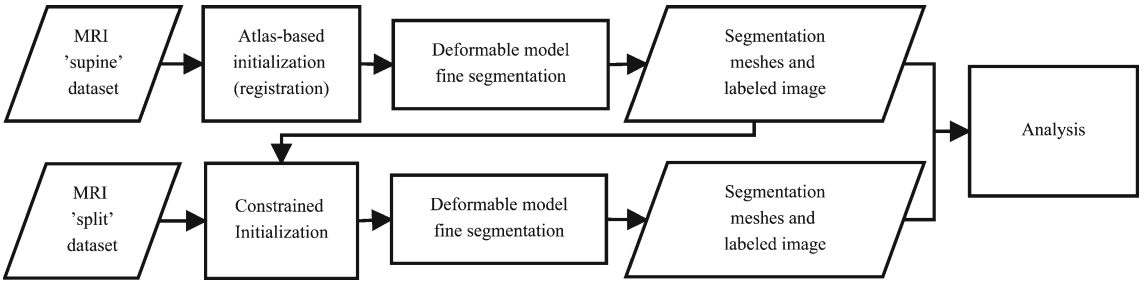

Fig. 2 Overall segmentation framework

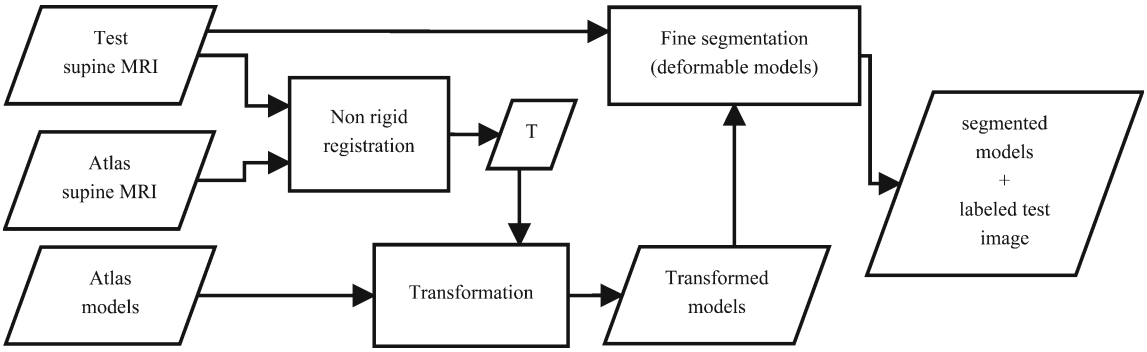

Fig. 3 Supine MRI segmentation pipeline

comparatively low resolution in these MRI to other standard MRI acquisitions was attributed to the large FOV and short acquisition time. Subjects were monitored and asked to remain as still as possible during the acquisition to avoid the formation of motion artifacts.

A subject was arbitrarily chosen among the 11 subjects as the 'atlas' and the femurs of the atlas in supine posture were segmented using an interactive segmentation performed by experienced researchers under the direct supervision of expert radiologists from the University Hospital of Geneva, Switzerland. The interactive segmentation used deformable models which were controlled by 'constraint points' manually placed by the operator. Using the same approach, all subject MRIs were segmented and the resulting segmented structures were referred to as the 'ground truth' for use in quantitative assessments.

Supine MRI segmentation

A detailed description of the supine MRI segmentation approach is illustrated in Fig. 3.

Atlas-based registration for segmentation initialization

For each subject's supine MRI, the MRI was registered to the atlas MRI using the volumetric registration toolset ElastiX [31]. The registration estimated the unknown non-rigid transform T between the fixed (atlas) (Fig. 4a) and the moving (subject MRI) images (Fig. 4b). Initially, an affine alignment was performed followed by a non-rigid B-Splines transformation to result in a registered subject MRI to the atlas. Both the transformations were optimized with standard gradient descent optimizer and a multi-resolution strategy with 3 resolution levels was used to avoid the local minima, where 100 iterations were applied at each level. For the B-Splines transform, a grid of $16 \times 16 \times 16$ voxels was used. These parameters were derived from trials which assessed the impact of the parameters with respect to the final segmentation results. The resulting T was used to transform the atlas's segmented meshes which were then used in the subsequent deformable models based segmentation of the subject MRI (see Fig. 4b).

Deformable models based segmentation

As shown in Fig. 2, the registration results provide initialization for a further segmentation, based in our case on deformable models (Fig. 3). In our previous work [20], we presented a segmentation method based on physically based deformable models. Models were represented as 2-simplex meshes [32] (dual of triangular meshes) with vertices regarded as lumped mass particles. Models evolved under the Newtonian law of motion and were driven by external image forces. The image forces guided the models toward boundaries which had

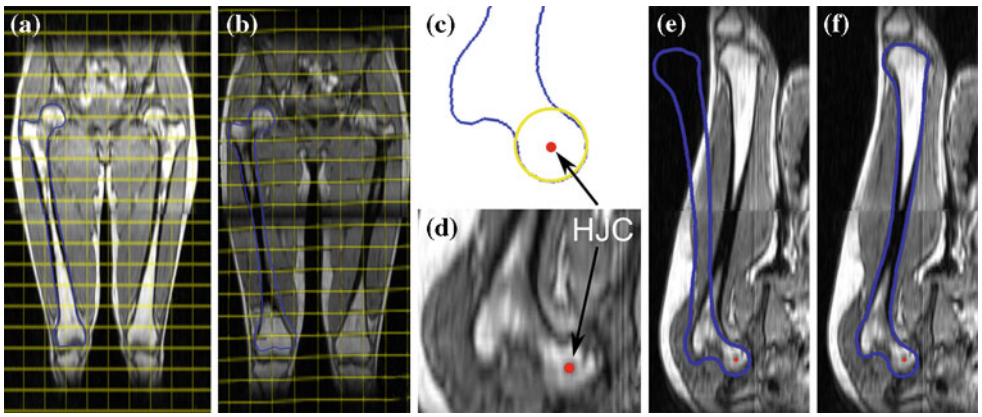

Fig. 4 Registration-based initializations for supine (**a**, **b**) and split (**c–f**) images. **a–b** non-rigid registration between **a** atlas and **b** subject's supine MRI: *blue* overlay represents the **a** atlas and **b** the transformed right femur with the computed transformation T; the *yellow grid* illustrates the non-rigid deformation. **c–f** model-to-image registration: the hip joint center (HJC) is estimated in **c** the supine segmented model by a sphere fitting (*yellow circle*) approach and on **d** the image by a mouse click on the center of the femoral head. The sought rigid transform M is constrained to be a rotation around the HJC with a small translation, as shown in (**e**) and (**f**)

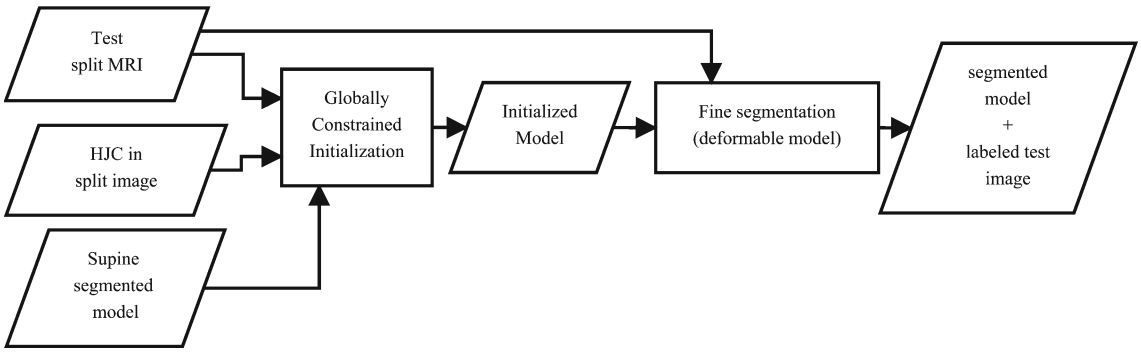

Fig. 5 Split MRI segmentation pipeline

(i) local intensity neighborhoods, denoted as intensity profiles (IP) [22,32], similar to pre-defined IPs, and (ii) expected gradient directions [9]. In our case, these pre-defined IPs were approximated from the atlas MRI. To cope with intensity variations between the IPs of different datasets, the robust normalized cross correlation (NCC) similarity measure was used:

$$NCC(p,q) = \frac{\sum_i (p_i - \bar{p})(q_i - \bar{q})}{\sqrt{\sum_i (p_i - \bar{p})^2 \sum_i (q_i - \bar{q})^2}} \quad (1)$$

where $p = \{p_1, \ldots, p_d\}$ and $q = \{q_1, \ldots, q_d\}$ are two IPs of same length and $\bar{p}$ and $\bar{q}$ are the mean of the samples p_i and q_i, respectively. Since the dual-posture MRI images were corrupted with artifacts, noise and low image resolution, the models evolution must be regularized to prevent false deformations. Regularization forces, based on smoothing and statistical shape models (SSM) of the evolving shapes [33], were applied, in which the SSM point correspondence was established with a template model-to-image registration procedure [20,34] from a training dataset of bone shapes (exclusive of the dancer data).

Split MRI segmentation

The split segmentation exploits a global initialization followed by the same supine deformable model segmentation as depicted in Fig. 5.

Constrained global initialization

Its fundamental idea relies on the use of shape and appearance of the segmented models from the supine MRI of the same subject, where the bone structure does not deform between the two postures and intensity neighborhoods in vicinity to the bone surface undergo minor variations compared to other anatomical regions. The initialization problem was thus reduced to a *rigid* model-to-image registration in which a model (segmented mesh from subject supine MRI) was

registered to the subject's split image by finding an unknown rigid transformation M, as illustrated in Fig. 4e, f.

The bone position in the split image was not a known prior, as each dancer performs a split with a different degree of 'bending' and positions herself in a preferred and different manner in the scanner. It is thus necessary to constrain the rigid registration. Our approach constraints the supine femur shape's rotation to be centered around its hip joint center (HJC), as shown in Fig. 4e, f. The HJC's position was approximated in the split image by a simple mouse click on a slice (Fig. 4d) as the center of the femoral head, and on the bone shape (Fig. 4c) by an automatic sphere fitting procedure [24]. Points used in the sphere fitting were defined only once on the atlas femur model. This constrained motion mimics the femur kinematics (ball-and-socket joint) and limits the transform parameter's search space. The rigid transform M also considered small isotropic translations of 1 mm around the HJC to account for the error in positioning the HJC in the image. The computation of M was formulated as the minimization of a functional f which expresses the degree of fitting of femur model x to the split MRI. The functional f uses the same similarity measure based on the NCC of intensity profiles (1), and the reference IPs, IP_i^{ref}, were then computed from the supine MRI:

$$f(M; x) = \sum_i NCC(IP_i(M(x)), IP_i^{ref}) \quad (2)$$

where $M(x)$ is the model transformed by the rigid transform M, i indicates the indices of the points of $M(x)$ within the image extents and IP_i is an IP extracted at point i. To minimize f, the differential evolution (DE) optimizer [35] was selected as it is a global and self-adaptive technique. Adopting the concepts from evolutionary algorithms, DE considers the transformation parameters vector (3 rotation angles and 3 translations) as an individual of a population which undergoes transformations through mutation, crossover and selection operations. DE was selected due to its robustness against the presence of local minima and it being not sensitive to the initialization. The chosen parameters for the DE were suggested in the work of [35]. In particular, we used the 'RAND1BIN' crossover scheme and set the number of generations to 100. With the completion of the DE-based initialization, a local minimization of the functional f based on the downhill simplex method [36] was finally conducted to refine the transform M.

Deformable models based fine segmentation

As with supine MRI, deformable models are applied as a fine segmentation using the aforementioned initialization with reference IPs computed from the supine MRI.

Results

Our proposed algorithm was evaluated with 10 female dancer datasets. All results were qualitatively and quantitatively measured against the ground truth, using well-known evaluation metrics that aggregates (i) Average symmetric surface distance (ASSD); (ii) Average symmetric root mean square surface distance (ASRSD); (iii) Maximum surface distance (MSD); and (iv) Volumetric overlap error (VOE) [37]. Most of these measures are based on the (asymmetric) 'surface distance' $SD(x,y)$ between meshes $x = \{x_1, \ldots, x_n\}$ and $y = \{y_1, \ldots, y_m\}$. SD is defined as $SD(x, y) = \sum_i d(x_i; y)/n$, where $d(x_i; y)$denotes the surface distance at point level and is computed as the distance in mm between point x_i and its projection on the surface of mesh y. The ASSD is one of the most commonly used measures [37] which we adopt as the reference measure.

Supine posture segmentation evaluation

Averaged results of the supine posture segmentation are shown in Table 1 for both the registration (initialization) and deformable model-based 'fine' segmentation. All the data were registered using the same atlas and registration parameters defined in section "Related work". The registration errors were as expected high and inconsistent (e.g., average ASSD of 5.86 ± 2.15 mm for both sides); however, the results in all cases were sufficient for its use as an initialization of the subsequent fine segmentation. Indeed, the fine segmentation resulted in significant improvements, e.g., VOE of 50.13% dropped to 17.18%. Figure 6 shows the differences between the two segmentation phases among the 10 subjects. The errors between the registration and fine segmentation results were in average improved by 75%, and the results were statistically significantly different (e.g., p-value = 0.0001 with a one-tailed Mann–Whitney rank test for left/right femur). More importantly, the variance between the subjects had even larger improvements of 83% thus suggesting the consistency and the reliability of the fine segmentation, even with not so accurate initializations. The use of SSM contributed to the robustness of the fine segmentation to bad initializations.

The quantitative findings are confirmed by the visual results, where Fig. 7 illustrates the accuracy of the proposed dual-posture segmentation, exemplified by subject 1 for which the registration error was the highest (ASSD of 10.29 mm) and subject 10 who had the lowest initialization errors (ASSD 3.73 mm). The visual differences between the fine segmentation and the ground truth are minor for both subjects. The overall performance of the fine segmentation results was ASSD of 1.48 ± 0.36 mm (average of left and right femurs). Comparative examples between the fine segmentation and the ground truth are shown in Fig. 8. In order

Table 1 Supine overall registration and fine segmentation errors (average ± standard deviation) for left and right femurs from 10 subjects

Bone	ASSD (mm)	ASRSD (mm)	MSD (mm)	VOE (%)
	Registration			
Right femur	5.66 ± 2.23	7.74 ± 3.41	26.18 ± 11.17	48.69 ± 9.48
Left femur	6.05 ± 2.08	8.07 ± 2.73	27.38 ± 7.48	51.57 ± 9.94
All	5.86 ± 2.15	7.90 ± 3.07	26.78 ± 9.32	50.13 ± 9.71
	Fine segmentation			
Right femur	1.27 ± 0.36	2.07 ± 0.54	9.38 ± 2.45	16.28 ± 2.98
Left femur	1.68 ± 0.37	2.65 ± 0.64	11.35 ± 2.01	19.69 ± 2.33
All	1.48 ± 0.36	2.36 ± 0.59	10.37 ± 2.23	17.98 ± 2.67

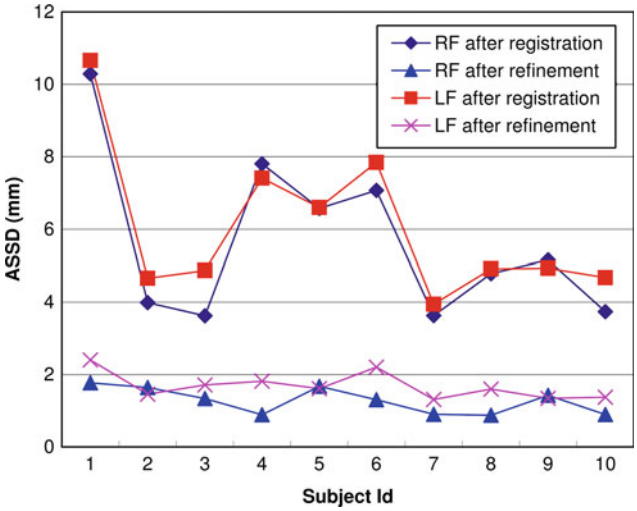

Fig. 6 Segmentation results errors for supine MRIs measured with ASSD for the registration (initialization) and fine segmentation phases. Both the right femur (RF) and left femur (LF) results of all 10 subjects are plotted

to study the largest error range, we compared all the segmentation models to their ground truth counterparts using the average SD at the point level (i.e., for each point of the segmentation model, the SD at point level was computed and averaged among the 10 subjects). This produced an error distribution over the bone, which was color-mapped for quantitative inspection (Fig. 9a). Largest errors were localized in the regions of the lesser (LT) and greater (GT) trochanters, and particularly the patellar surface (PS) and the condyles (C). Errors in C and PS regions were explained by the low image intensity (see e.g., Fig. 7a in the knees section) and large slice thickness (5 mm) which hindered the segmentation of regions parallel to the axial plane. The LT and GT are regions where the femur anatomy is more complex and hampered by noise, and thus the SSMs used in the fine segmentation were not always able to perfectly express the variability. This resulted in lower segmentation accuracy in relation to other regions, which is consistent with other studies [38]. Nevertheless, the error distribution analysis showed that 80% of errors were below 2 mm meaning that large errors did not excessively cover large portions of the bone.

Split posture segmentation evaluation

The results of split segmentation are reported in Table 2 with visual comparisons in Fig. 10. These results highlight the capabilities of the constrained global initialization (GI) to yield initial models that match closely to the ground truth (e.g., worst subject was 7 with ASSD of 4.57 mm for right femur). As in the supine data, the fine segmentation has again significantly improved the overall ASSD, from 2.22 ± 1.10 to 1.30 ± 0.26 mm (p-value = 0.024). Figure 11 typically illustrates this improvement between initialization and fine segmentation. As with the supine results, the split segmentation resulted in satisfactory agreement to the ground truth, in low standard deviation (0.26 mm), which highlighted the precision of the approach, and in a similar error distribution (Fig. 9b). Compared to the supine results, the overall accuracy was better but some high errors were observed in other highly localized regions, such as the intercondylar fossa (Fig. 9b).

Discussions and future work

Our proposed dual-posture MRI segmentation resulted in reliable and robust segmentations of the femurs with clinical images of professional ballet dancers. Our quantitative assessment demonstrated that our approach was able to segment femurs with an average error (split and supine) of 1.39 ± 0.31 mm, which is sufficient for use in extreme motion analysis and diagnosis using these data. In fact, all final segmentation errors for both supine and split postures were below the value of 1.5 mm, error which has been reported as satisfactory for bone computer-aided applications [39]. Moreover, it is worth mentioning that in some subjects, due to the low resolution MRI, the ground truth that was manually delineated by the expert was error-prone (e.g., visual

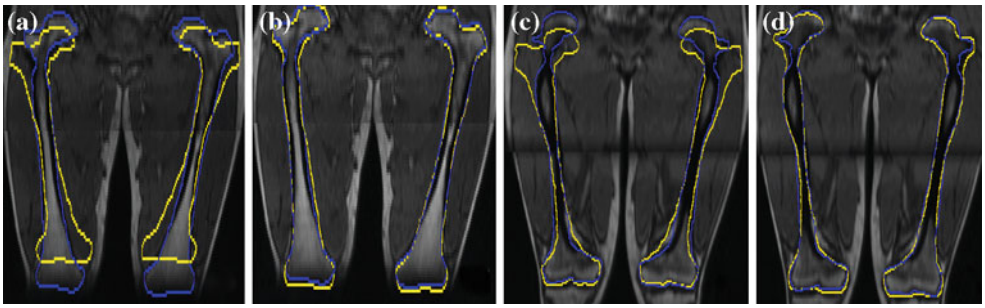

Fig. 7 **a**, **c** Registration (*yellow*) versus ground truth (*blue*) results for subject 1 and 10, respectively, in supine MRI. **b**, **d** Fine segmentation (*yellow*) versus ground truth (*blue* results for subject 1 and 10, respectively

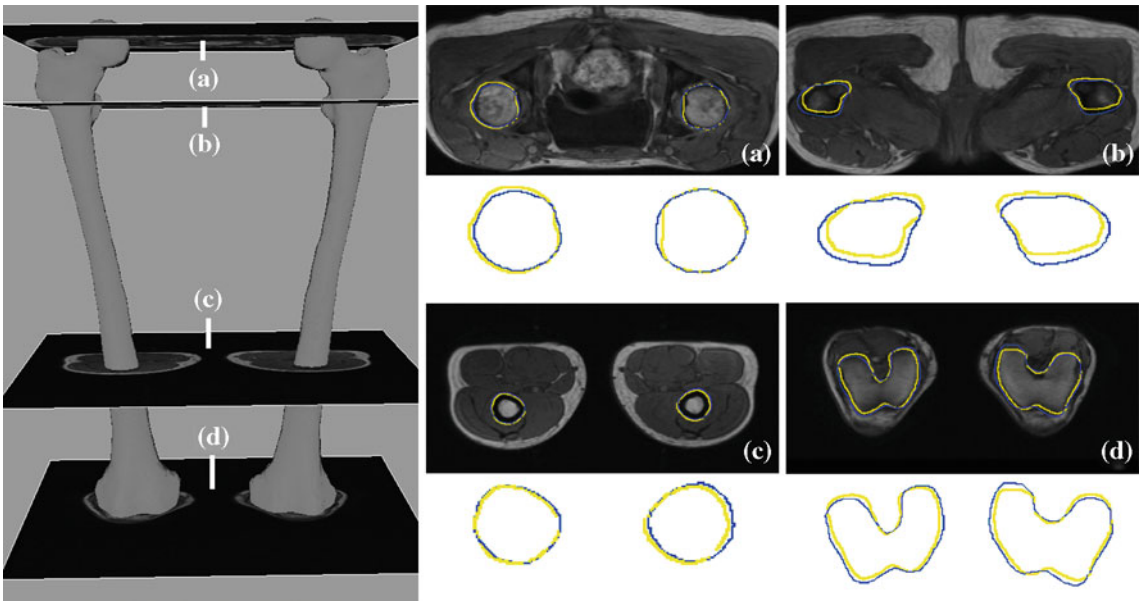

Fig. 8 Comparison between the ground truth (*yellow*) and the fine segmentation (*blue*) result in a supine MRI data with zoomed overlays

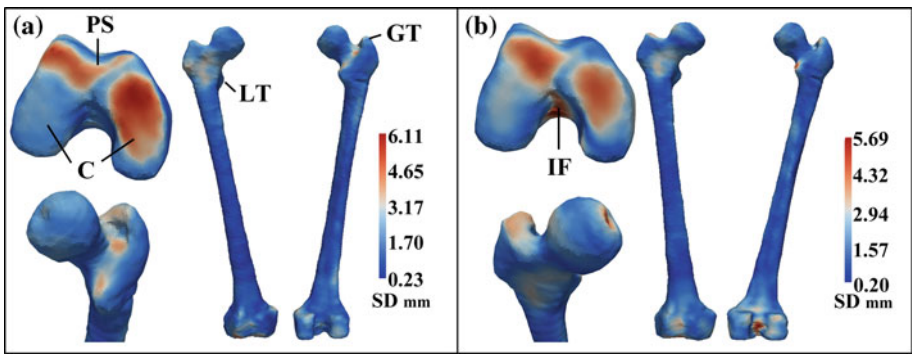

Fig. 9 Average surface distance (SD) error distribution over a standard right femur shape. A color mapping of the error on the shape reveals the largest errors on the regions of the patellar surface (PS), the greater (GT) and lesser trochanters (LT), condyles (C) and intercondylar fossa (IF) for the **a** supine and **b** split final results

assessment of the ground truth of trochanters in Fig. 8b), resulting in lower segmentation evaluation scores. The consistency of the split segmentation in relation to the supine results suggested that our algorithm was adequate in using the validated supine posture segmentation result for assisting the segmentation of unique split posture protocol. Our algorithm was not limited to the use of deformable models as presented in this study, where the segmentation of the femur in the *supine* MRI could be derived with other segmentation approaches (e.g., [13,26]).

The low accuracy in the atlas-based registration was attributed to the use of an atlas which has large differences in intensity distributions and anatomical variations when compared to subject datasets. Furthermore, the registration attempted

Table 2 Split overall constrained initialization and fine segmentation errors (average ± standard deviation) for left and right femurs from 10 subjects

Bone	ASSD (mm)	ASRSD (mm)	MSD (mm)	VOE (%)
	Constrained initialization			
Right femur	2.28 ± 1.11	3.33 ± 1.47	12.32 ± 4.99	25.02 ± 9.20
Left femur	2.16 ± 1.09	3.16 ± 1.40	12.24 ± 3.60	24.59 ± 9.22
All	2.22 ± 1.10	3.24 ± 1.43	12.28 ± 4.29	24.80 ± 9.21
	Fine segmentation			
Right femur	1.19 ± 0.20	1.89 ± 0.24	8.68 ± 1.52	16.05 ± 2.21
Left femur	1.41 ± 0.33	2.25 ± 0.46	10.38 ± 1.98	17.6 ± 3.02
All	1.30 ± 0.26	2.07 ± 0.35	9.53 ± 1.75	16.83 ± 2.62

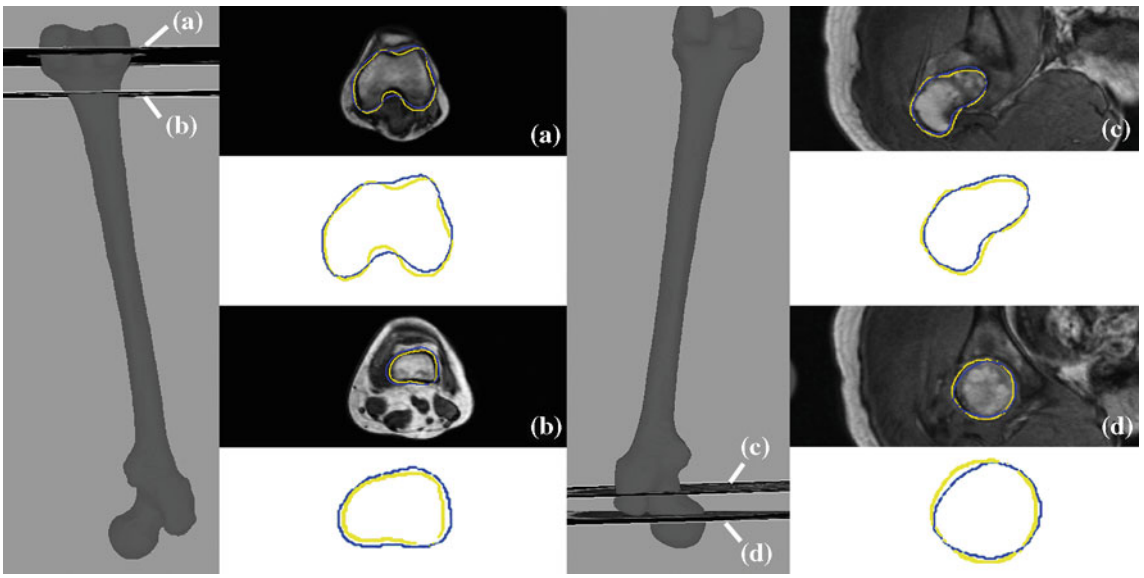

Fig. 10 Comparison between the ground truth (*yellow*) and the fine segmentation (*blue*) in split MRI with zoomed overlays. **a**, **b** and **c**, **d** are respectively from a right and left split segmentations

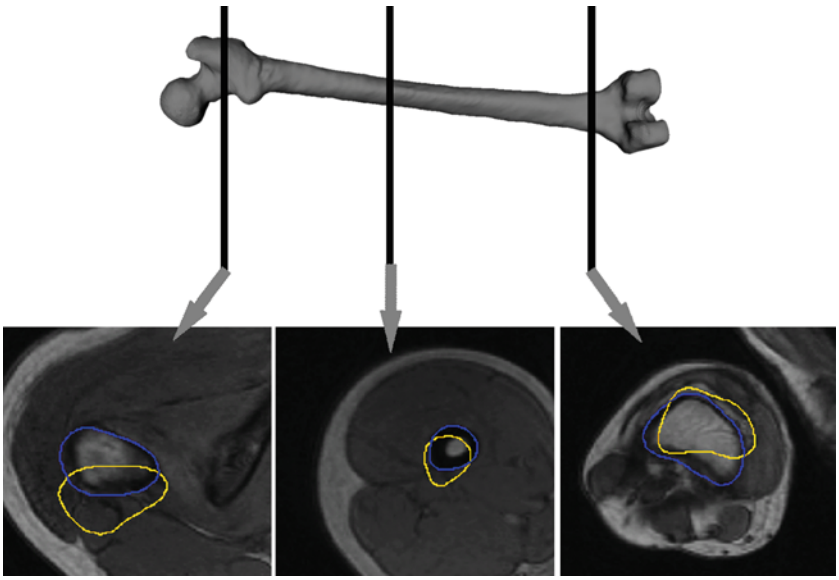

Fig. 11 Example of worst case of split initialization (*yellow*) compared with the fine segmentation results (*blue*), which are significantly better (decrease of ASSD from 4.57 to 1.03 mm)

to register MRI that were mostly composed of soft tissues, thus the registration emphasized the similarity among the soft tissues rather than the femur. Nevertheless, the atlas used was based on a single subject scan and was able to produce a satisfactory initialization for this study. This was possible because all the subject scans were from a same population group, sharing same gender, age group, and similar physical attributes (e.g., height). We anticipate that with the addition of statistical properties in the construction of the atlas, e.g., atlas averaging via clustering of the registered data [40], the initialization of the segmentation should be improved, thus leading to further improvements in the segmentation.

The segmentation of a split posture could theoretically follow the same procedures as in the supine segmentation, i.e., registration to an atlas for initialization. However, in our assessment, a selection of a subject for use as the atlas in split postures failed due to the ubiquitous inter-subject variations between the split images (unpredictable variations of femur rotation angles and surrounding soft tissue deformations), which strongly affected the registration process. Similarly, an intra-subject registration between the supine and split MRI remained even more problematic due to the larger rotation variations between the two postures.

The proposed algorithm expedites the tedious and complex (especially the proximal femur) manual segmentations of the femur bone in MRI images. Our algorithm requires in average 11 min to process the dual-posture MRI (segmenting both the left and the right femurs in supine and split images) using modest PC specifications (3.40 GHz P4; 2 GB RAM). This measured time encompasses both the registration (non-rigid and model-to-image) and deformable models based segmentation. This time is expected to decrease significantly with code optimization and better PC configurations. In contrast, the average time of 24 min was measured in the manual delineation of the same MRIs for the ground truth data construction using the supervised segmentation approach (see Section on *Ground Truth Construction*).

Our segmentation of the dual-posture MRI is fully automatic apart from the manual placement of the HJC in the image. Existing methods to automatically detect the HJC that rely on edge detectors, such as Hough transforms [41] failed to provide adequate results. This was due to the low image resolution and weak gradients at the femoral head boundaries. We proposed thus a simple yet efficient manual intervention, requiring only a single click approximation and we are currently working on automatic solutions to replace this manual task.

Future work will also involve the segmentation of other anatomical structures, such as the hip bones, or pathological bony structures such as oblique/complete fractures or necrotic femoral heads [26]. Furthermore, a more thorough analysis of extreme motion effects in professional dancers will be conducted. Finally, other less extreme and more common motions will be studied in order to target a larger and more diversified population of (sportive) people.

Conclusions

This study presented an automated MRI segmentation of the femur from dual-posture MRI for extreme motion analysis of professional ballet dancers. With our novel exploitation of the rigid properties of the bone structure (no change between supine and split postures), we demonstrated the effectiveness of our segmentation algorithm in delineating the dual-posture images. Although our study targets the particular population of professional ballet dancers, the proposed methodology is applicable to the study of other hip motion as long as images of the various postures are available. The supine-split motion was chosen because it provides an extreme case scenario to assess the efficiency and robustness of the proposed framework.

Acknowledgments This work was supported by the 3D Anatomical Human Project (MRTN-CT-2006-035763) funded by the European Union. We like to thank our partners, the University Hospital of Geneva and all the ballet volunteers from the Great Theater of Geneva, for their valuable contributions and expertise.

References

1. Pollard TCB, Gwilym SE, Carr AJ (2008) The assessment of early osteoarthritis. J Bone Joint Surg [Br] 90(4):411–421
2. Assassi L, Charbonnier C, Schmid J, Volino P, Magnenat-Thalmann N (2009) From mri to anatomical simulation of the hip joint. Comput Anim Virtual Worlds J, Spec Issue Physiol Hum: 53–66
3. Charbonnier C, Assassi L, Volino P, Magnenat-Thalmann N (2009) Motion study of the hip joint in extreme postures. Vis Comput 25(9):873–882
4. Ganz R, Parvizi J, Beck M, Leunig M, Nötzli H, Siebenrock K (2003) Femoroacetabular impingement: a cause for osteoarthritis of the hip. Clin Orthop Relat Res 417:112–120
5. Pfirrmann CWA, Mengiardi B, Dora C, Kalberer F, Zanetti M, Hodler J (2006) Cam and pincer femoroacetabular impingement: Characteristic mr arthrographic findings in 50 patients. Radiology 240(3):778–785
6. Gilles B, Kolo-Christophe F, Magnenat-Thalmann N, Becker C, Duc S, Menetrey J, Hoffmeyer P (2009) MRI-based assessment of hip joint translations. J Biomech 42(9):1201–1205
7. Fripp J, Crozier S, Warfield S, Ourselin S (2007) Automatic segmentation of the bone and extraction of the bone-cartilage interface form magnetic resonance images of the knee. Phys Med Biol 52:1617–1631
8. Li W, Abram F, Beaudoin G, Berthiaume M, Pelletier J, Pelletier J (2008) Human hip joint cartilage: MRI quantitative thickness and volume measurements discriminating acetabulum and femoral head. IEEE Trans Biomed Eng 55(12):2731–2740
9. Gilles B, Moccozet L, Magnenat-Thalmann N (2006) Anatomical modelling of the musculoskeletal system from mri. In: Proc. MICCAI, LNCS, vol 4190. Springer, Berlin, pp 289–296

10. Lorigo LM, Faugeras OD, Grimson WEL, Keriven R, Kikinis R (1998) Segmentation of bone in clinical knee mri using texture-based geodesic active contours. In: Proc. MICCAI, LNCS, vol 1496. Springer, London, pp 1195–1204
11. Snel J, Venema H, Grimbergen C (2002) Deformable triangular surfaces using fast 1-D radial Lagrangian dynamics-segmentation of 3-D MR and CT images of the wrist. IEEE Trans Med Imag 21:888–903
12. Hoad C, Martel A (2002) Segmentation of mr images for computer-assisted surgery of the lumbar spine. Phys Med Biol 47(19):3503–3517
13. Dalvi R, Abugharbieh R, Wilson D, Wilson D (2007) Multi-contrast mr for enhanced bone imaging and segmentation. In: Proc. EMBC, pp 5620–5623
14. Kang Y, Engelke K, Kalender W (2003) A new accurate and precise 3-d segmentation method for skeletal structures in volumetric ct data. IEEE Trans Med Imag 22(5):586–598
15. Reginster J (2002) The prevalence and burden of arthritis. Rheumatology 41(12):3–6
16. McPherson A, Kärrholm J, Pinskerova V, Sosna A, Martelli S (2005) Imaging knee position using MRI, RSA/CT and 3D digitisation. J Biomech 38(2):263–268
17. Lane NE, Buckwalter JA (2000) Exercise and osteoarthritis. Curr Opin Orthop 11(1):62–65
18. Galois L, Etienne S, Grossin L, Watrin-Pinzano A, Cournil-Henrionnet C, Damien L, Netter P, Mainard D, Gillet P (2004) Dose-response relationship for exercise on severity of experimental osteoarthritis in rats: a pilot study. Osteoarthr Cartil 12(10):779–786
19. Kress I, Siebenrock K, Werlen S, Mamisch T (2009) Sports-related alterations of the hip joint and correlation to typical findings in femuro-acetabular impingement: Mr findings in 50 elite karate fighters. In: European Congress on Radiology, vol 19, p 64
20. Schmid J, Magnenat-Thalmann N (2008) MRI bone segmentation using deformable models and shape priors. In: Proc. MICCAI, LNCS, vol 5241. Springer, Berlin, pp 119–126
21. Lamecker H, Seebaß M, Hege HC, Deuflhard P (2004) A 3d statistical shape model of the pelvic bone for segmentation. In: Proc. SPIE, vol 5370, pp 1341–1351
22. Seim H, Kainmüller D, Heller M, Lamecker H, Zachow S, Hege HC (2008) Automatic segmentation of the pelvic bones from ct data based on a statistical shape model. In: Eurographics workshop on visual computing for biomedicine, eurographics association, pp 93–100
23. Pettersson J, Knutsson H, Borga M (2006) Automatic hip bone segmentation using non-rigid registration. In: Proc. ICPR, vol 3, pp 946–949
24. Ehrhardt J, Handels H, Wegner T, Strathmann B, Plotz W, Poppl S (2000) An anatomical atlas to support the virtual planning of hip operations. Stud Health Technol Inform 77:1226–1230
25. Kratky J, Kybic J (2008) Three-dimensional segmentation of bones from ct and mri using fast level sets. In Proc. SPIE, vol 6914, pp 47–57
26. Zoroofi RA, Sato Y, Nishii T, Sugano N, Yoshikawa H, Tamura S (2004) Automated segmentation of necrotic femoral head from 3d MR data. Comput Med Imag Graph 28(5):267–278
27. Scheys L, Loeckx D, Spaepen A, Suetens P, Jonkers I (2009) Atlas-based non-rigid image registration to automatically define line-of-action muscle models: a validation study. J Biomech 42(5):565–572
28. Bourgeat P, Fripp J, Stanwell P, Ramadan S, Ourselin S (2007) Mr image segmentation of the knee bone using phase information. Med Image Anal 11(4):325–335
29. Rifai H, Bloch I, Hutchinson S, Wiart J, Garnero L (2000) Segmentation of the skull in mri volumes using deformable model and taking the partial volume effect into account. Med Image Anal 4(3):219–233
30. Gilles B, Perrin R, Magnenat-Thalmann N, Valle JP (2004) Bone motion analysis from dynamic mri: acquisition and tracking. In: Proc. MICCAI, LNCS, vol 3217. Springer, Berlin, pp 942–949
31. Klein S, Staring M, Pluim PJ (2007) Evaluation of optimization methods for nonrigid medical image registration using mutual information and b-splines. IEEE Trans Image Process 16(12):2879–2890
32. Delingette H (1999) General object reconstruction based on simplex meshes. Int J Comput Vis 32(2):111–146
33. Cootes TF, Hill A, Taylor CJ, Haslam J (1993) The use of active shape models for locating structures in medical images. In: Proc. IPMI, vol 687. Springer, pp 33–47
34. Heimann T, Meinzer HP (2009) Statistical shape models for 3D medical image segmentation: a review. Med Image Anal 13(4):543–563
35. Storn R, Price K (1995) Differential evolution—a simple and efficient adaptive scheme for global optimization over continuous spaces. Tech. Rep. TR-95-012, International Computer Science Institute
36. Nelder J, Mead R (1965) A simplex method for function minimization. Comput J 7(4):308–313
37. Heimann T, van Ginneken B, Styner M, Arzhaeva Y, Aurich V, Bauer C, Beck A, Becker C, Beichel R, Bekes G et al (2009) Comparison and evaluation of methods for liver segmentation from CT datasets. IEEE Trans Med Imag 28:1251–1265
38. Barratt DC, Chan CS, Edwards PJ, Penney GP, Slomczykowski M, Carter TJ, Hawkes DJ (2008) Instantiation and registration of statistical shape models of the femur and pelvis using 3D ultrasound imaging. Med Image Anal 12(3):358–374
39. Livyatan H, Yaniv Z, Joskowicz L (2003) Gradient-based 2-D/3-D rigid registration of fluoroscopic X-ray to CT. IEEE Trans Med Imag 22(11):1395–1406
40. Zhang L, Hoffman E, Reinhardt J (2006) Atlas-driven lung lobe segmentation in volumetric X-ray CT images. IEEE Trans Med Imag 25(1):1–16
41. Cao M, Ye C, Doessel O, Liu C (2006) Spherical parameter detection based on hierarchical Hough transform. Pattern Recogn Lett 27(9):980–986